

Ultra High Molecular Weight Polyethylene: optical features at millimeter wavelengths

G. D'Alessandro^a, A. Paiella^a, A. Coppolecchia^a, M.G. Castellano^b, I. Colantoni^c, P. de Bernardis^a, L. Lamagna^a, S. Masi^a

^a*Dipartimento di Fisica, Università di Roma La Sapienza, P.le A. Moro 2, 00185 Roma, Italy*

^b*Istituto di Fotonica e Nanotecnologie - CNR, Via Cineto Romano 42, 00156 Roma, Italy*

^c*Istituto di Fotonica e Nanotecnologie - CNR, Via Cineto Romano 42, 00156 Roma, Italy; Now at Dublin Institute for Advanced Studies, School of Cosmic Physics Astronomy and Astrophysics Section, 31 Fitzwilliam Place, D02 XF86, Dublin, Ireland*

Abstract

The next generation of experiments for the measurement of the Cosmic Microwave Background (CMB) requires more and more the use of advanced materials, with specific physical and structural properties. An example is the material used for receiver's cryostat windows and internal lenses. The large throughput of current CMB experiments requires a large diameter (of the order of 0.5m) of these parts, resulting in heavy structural and optical requirements on the material to be used. Ultra High Molecular Weight (UHMW) polyethylene (PE) features high resistance to traction and good transmissivity in the frequency range of interest. In this paper, we discuss the possibility of using UHMW PE for windows and lenses in experiments working at millimeter wavelengths, by measuring its optical properties: emissivity, transmission and refraction index. Our measurements show that the material is well suited to this purpose.

Keywords: Far infrared and millimeter Wavelengths; Polymer material; Optical features; Astronomy and astrophysics.

1. Introduction

The survey sensitivity of CMB experiments is currently pursued increasing the number of radiation modes detected, either using large-format arrays of

single-mode detectors or using arrays of multi-moded detectors. In both cases, the large optical throughput of the instrument requires large optical elements. The first element (skywise) of the receiver optical train is the cryostat window. Its optimization is crucial because it represents the first filter for the radiation, therefore must have a high transmission in the frequency bands of the experiment and, at the same time, must withstand without bending too much the large inwards force due to external pressure and internal vacuum.

Nowadays, High Density Polyethylene (HDPE) is widely used for cryostat windows [1, 2, 3, 4, 5, 6] and lenses in the millimeter-waves frequency range of interest here [6, 7, 8, 9]. UHMW PE is a kind of thermoplastic polyethylene. It has extremely long chains of polyethylene, all aligned in the same direction. The molecule forming UHMW chains is heavier than that of HDPE, and this makes the UHMW stronger and easier to be machined [10, 11]. The tensile strength of UHMW PE is twice that of HDPE, therefore it represents a good candidate for replacing HDPE.

Although some experiments devoted to the measurements of the CMB, like the Atacama Cosmology Telescope, CLASS, and BRAIN pathfinder, already used this material for their optical components [9, 12, 13, 14, 15], direct measurements of its most important optical characteristics cannot be found in the literature yet. In this paper we report measurements of emissivity, transmission and refraction index for UHMW PE, providing useful data for the design of new CMB experiments and other optical instruments for mm-wave measurements.

2. Mechanical characteristics and simulations

The tensile strength of UHMW PE is ~ 40 MPa, while that of HDPE is ~ 20 MPa. In order to evaluate the impact of this characteristics on the mechanical performance of large windows, we performed a load simulation of a large diameter window, for both materials, using a finite element simulator¹.

¹Solidworks in this case, but other software, such as ANSYS and COMSOL MULTI-PHYSICS give the same results

The simulated window has a diameter of 50 cm, a thickness of 2.5 cm, and its temperature has been set at 300 K (room temperature). The pressure difference from top to bottom is 1000 mbar². As expected, the simulations Figure 1 confirm that the UHMW window deformats less. This means that it is possible to use less material in order to have the same mechanical performance of the HDPE, see Tab. 1. Less material means less weight, and better transmission. Thanks to this mechanical feature, each secondary machining on the surface, such as anti-reflection coating, is easier and the risk of damage to the material is reduced.

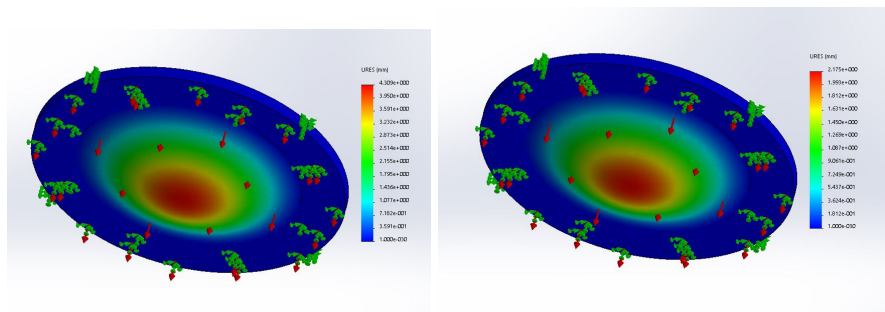


Figure 1: Finite elements simulation performed with ANSYS. The simulated window has a diameter of 50 cm, a thickness of 2.5 cm, and its temperature has been set at 300 K (room temperature). The windows are subjected to pressure of 1000 mbar and show a displacement of 4.3 mm for the HDPE and 2.2 mm for the UHMW

2.1. Deformation vs. thickness simulations

We use ANSYS software to show the deformation for three different cryostat windows, with diameter of 10 cm, 25 cm and 50 cm, as a function of thickness. We obtain results showed in Tab. 1.

The results in table shows how it is possible to reduce the thickness of windows from 25 mm to 20 mm, for each diameter, obtaining the same displacement and increasing the transmissivity, as it showed in Figure 7.

²Usually the internal cryostat pressure is $\sim 10^{-6} mbar$

diameter	thickness	deformation UHMW	deformation HDPE
[cm]	[cm]	[mm]	[mm]
50	1.0	14	19
50	2.0	4.0	7.9
50	2.5	2.2	4.3
25	1.0	2.0	3.9
25	2.0	0.3	0.6
25	2.5	0.2	0.3
10	1.0	0.07	0.1
10	2.0	0.01	0.03
10	2.5	0.003	0.02

Table 1: Displacements evaluate by using finite element simulations for three different cryostat window, subjected to 1000 mbar of pressure as a function of thickness.

3. Emissivity

The emissivity of the optical components is crucial because it represents part of the background power incident on the detectors and part of the optical load on the fridge of the cryogenic system.

The design of the detectors is strictly correlated with the background power, as well as the performance of the fridge depends on the optical load. A typical emissivity for the optical elements working at millimeter wavelengths is around few percent [16, 17, 18]. The direct measurement of the emissivity is not simple, since the quantity which we want to measure is small and it is easy that the experimental setup is dominated by systematics.

In order to estimate the UHMW emissivity, we build a setup like in [16]: a disk of UHMW, thickness of 10 mm, surrounded by a copper crown, which is, in turn, surrounded by an Aluminum ring, is suspended in air through some kevlar fibers, in order to thermally insulate the UHMW from its metal support. The aluminum ring is equipped with a number of evenly spaced heaters, which allow to control the temperature, while the disk of UHMW is equipped with two

thermometers PT100: one at the center and one near the copper crown. Figure 2 shows this setup. We verified, with dedicated tests, that the PT100 which is placed at the center of the UHMW disk, does not corrupt the measurement.



Figure 2: The UHMW disk is surrounded by a copper crown, needed to improve the thermalization. The copper crown is surrounded by an aluminum ring where a number of heaters is placed. The heaters allow to heat the UHMW and the temperature is monitored by two thermometers: one located at the center and the second located on the edge of the UHMW disk. The aluminum ring, to which the copper crown and the UHMW disk are anchored, is suspended in air through some kevlar fibers.

3.1. Instrumental setup

For this measurement, the instrumental setup is composed of low temperature detectors, in particular kinetic inductance detectors (KIDs) [19, 20], and therefore of a cryogenic system, equipped with a dedicated optical system, and the readout electronics.

The sample is placed in such a way that the signal coming from it is chopped with a blackbody at 300K (Eccosorb sheet) before entering in the cryostat, the Eccosorb sheet is glued to Aluminum sheet and the temperature is controlled with a PID system by using a PT100 thermometer and resistor like heater. The bias and the readout signals of the detector are monitored through a dedicated electronics, which include a frequency synthesizer, a signal splitter, an IQ mixer demodulator, a low noise amplifier, a warm amplifier, and an ADC. Figure 3 shows the scheme of this measurement setup.

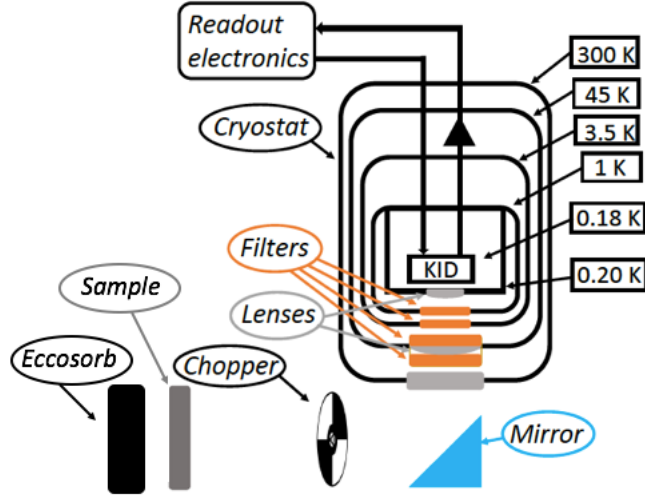


Figure 3: Scheme of the measurement setup used for the emissivity. The signal coming from the sample is chopped with a blackbody at 300 K and reflected in the cryostat by a 45° mirror. Inside the cryostat, the signal passes through the cryostat optical system and illuminates the detectors. The bias and the readout signals of the detector are monitored through a dedicated electronics.

3.1.1. Detectors

The detectors consist of two single pixel KIDs, built on $1\text{ cm} \times 1\text{ cm}$, $300\text{ }\mu\text{m}$ thick, high-quality (FZ method), intrinsic Silicon wafer, with high resistivity ($\rho > 10\text{ k}\Omega\text{ cm}$) and double side polished. The 90 GHz KID is a TiAl bilayer 10 nm thick Titanium + 25 nm thick Aluminum, while the 150 GHz KID is in Aluminum 25 nm thick. For both the detectors, the feedline is a coplanar waveguide, matched to $50\text{ }\Omega$.

The absorber of the 90 GHz KID is a standard meandered line, while that of the 150 GHz KID is a III order Hilbert curve. For both the detectors, the capacitor has the interdigitated geometry, designed in order to guarantee the lumped condition, and to have a resonance frequency around 1 GHz for the 90 GHz KID, and 2 GHz for the 150 GHz KID. Figure 4 shows the designs of the 90 GHz and 150 GHz KID.

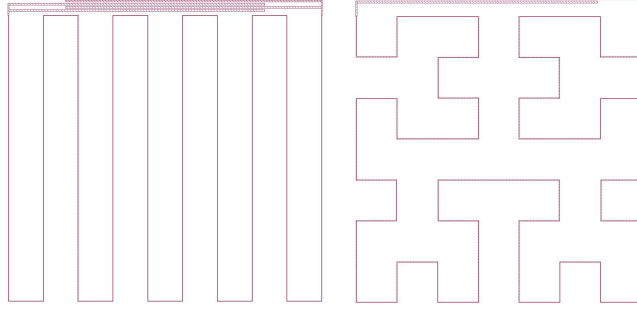


Figure 4: Designs of the 90 GHz (*left panel*) and of the 150 GHz (*right panel*) KID.

The detectors are fabricated at the Istituto di Fotonica e Nanotecnologie (IFN) of the Consiglio Nazionale delle Ricerche (CNR), in Rome [21].

The 90 GHz KID has a critical temperature $T_c = (812 \pm 24)$ mK and the noise equivalent temperature on the detector is $\text{NET} = (6.94 \pm 0.73)$ mK/ $\sqrt{\text{Hz}}$ [22]. The 150 GHz KID has a critical temperature $T_c = (1.32 \pm 0.04)$ K and the noise equivalent temperature on the detector is $\text{NET} = (0.909 \pm 0.095)$ mK/ $\sqrt{\text{Hz}}$.

3.1.2. Cryogenic system

KIDs are low temperature detectors, they need to be cooled below the critical temperature of the superconducting film in order to work. The optimal choice is at least $T \lesssim T_c/6$.

The cryogenic system is a three-stage cryostat composed of a pulse tube cryocooler, a $^3\text{He}/^4\text{He}$ fridge, and a dilution refrigerator. This system is able to reach a base temperature of 136 mK, under an optical loading of about 14 μW , for about 7 hours.

3.2. Measurements

For the setup described before, the signal is

$$S = \mathcal{R} \{ \epsilon_{\text{ecc}} [T_{\text{amb}} (t_{\text{UHMW}} + r_{\text{UHMW}}) - T_{\text{cho}}] + \epsilon_{\text{UHMW}} T_{\text{UHMW}} \} \quad (1)$$

where \mathcal{R} is the system responsivity in V/K, while t_{UHMW} and r_{UHMW} are the UHMW transmissivity and reflectivity, respectively, ϵ_{ecc} is the Eccosorb emis-

sivity. The product $\mathcal{R}\epsilon_{\text{ecc}}$ is calibrated by removing the UHMW and placing an Eccosorb plate, cooled at $T_N = 77.8$ K, behind the chopper, in this case the signal is

$$S_{\text{cal}} = \mathcal{R} [\epsilon_{\text{ecc}} (T_N - T_{\text{cho}})] . \quad (2)$$

The Eccosorb emissivity is estimated by measuring the transmissivity and the reflectivity of an Eccosorb slabs, using a high-power source: a 150 GHz Gunn oscillator. We obtained $\epsilon_{\text{ecc}} = 0.972 \pm 0.002$. At this point, the UHMW emissivity, ϵ_{UHMW} , is measured by fitting the trend of S/\mathcal{R} with the UHMW temperature, T_{UHMW} , eq. (1), see Figure 5. Tab. 2 collects the values of the responsivities and the results of the fits found for the two detectors working at 90 GHz and 150 GHz. The integration time are around 1 hour for both measurements.

f [GHz]	\mathcal{R} [mV/K]	$\sigma_{\mathcal{R}}$ [mV/K]	ϵ [%]	σ_{ϵ} [%]
90	0.72	0.01	2.1	1.3
150	0.723	0.005	2.9	0.4

Table 2: Values of the system responsivities and results of the linear fit on the trend of S/\mathcal{R} with the UHMW temperature, for the two detectors working at 90 GHz and 150 GHz.

4. Transmission

The transmission at millimeter wavelengths is a crucial property because it discriminates if a material can or can not be used. A proper material, for both the cryostat window and the lenses, must have a transmission near 100 %, in such a way that the optical losses, through these elements, are negligible. Nowadays, the most used material, which satisfies this requirement, is the HDPE [23, 24].

We performed transmission measurements on HDPE and UHMW samples with different thicknesses, and without any anti-reflection coating treatments.

4.1. Instrumental setup

For this measurement, the instrumental setup is composed of a Martin Puplett Interferometer (MPI), a Hg-Lamp (blackbody at 4000 K) and an Eccosorb

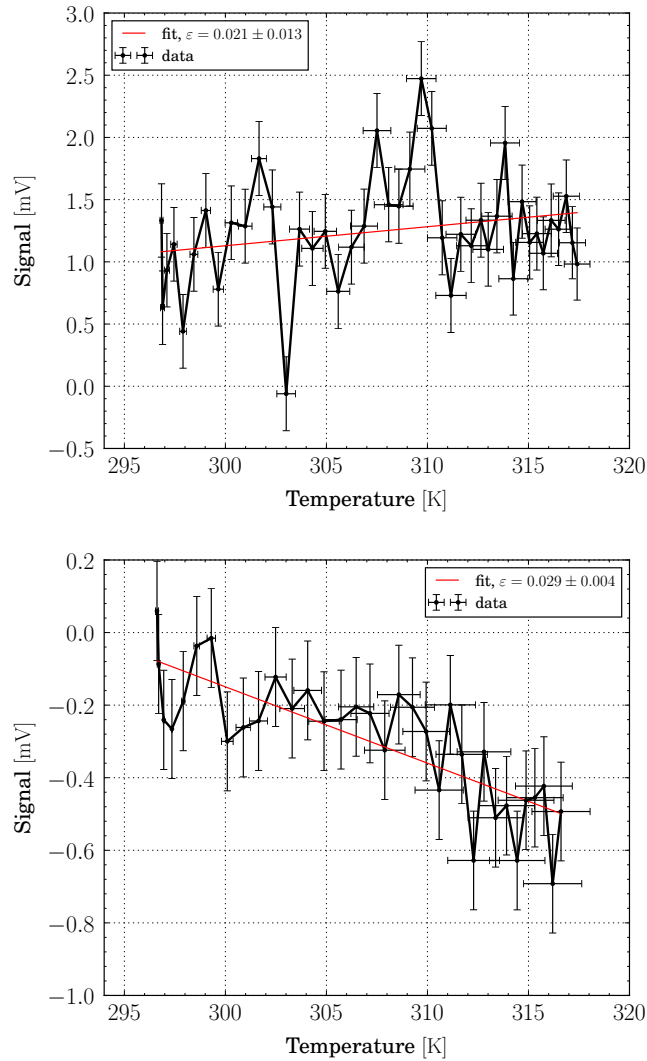


Figure 5: Measured intensity as a function of the UHMW temperature for the 90 GHz (*top panel*) and 150 GHz (*bottom panel*) detector.

sheet (blackbody at 300 K) as sources, and a Golay cell as detector. The Golay cell has a quartz lens which is a low-pass filter at 1 THz. The Wire Grids used for the MPI starting to be ideal at 90 GHz so we decided to show the measurement from 150 GHz to 870 GHz.

In the inputs of the MPI, we placed the Hg-Lamp and the Eccosorb sheet at room temperature, while the samples are placed directly in front of the Golay cell. The input signal is modulated at 3.6 Hz through a chopper, and it is collimated on the detector through a Quartz lens, which acts as a 1 THz low-pass filter as well. The output signal is demodulated through a Lock-in amplifier.

Figure 6 shows a scheme of this setup, which is the same used in [25], in such a way that all the systematics are under control [16, 25, 26, 27].

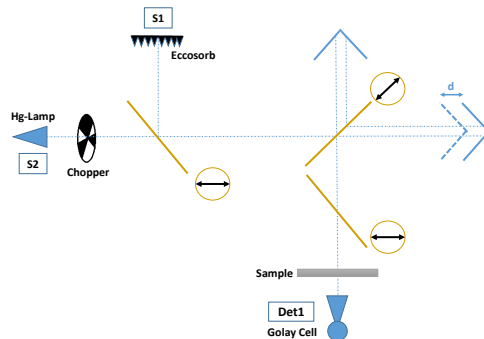


Figure 6: Scheme of the measurement setup used for the transmissivity and for the refraction index. The sample is placed between the last wire grid of the MPI and the detector, for the measurement of the transmission, while it is placed between the beam splitter and one of the two roof mirrors, in order to increase the phase shift, for the measurement of the refraction index.

4.2. Measurements

In order to measure the transmissivity, we need to perform two measurements: with and without the sample. For each measurement, we acquired a single interferogram, around 15 minutes of integration time, and we calculate the associated power spectrum by using a discrete fast Fourier transform algorithm. The spectrum obtained with the sample is normalized to that obtained without the sample. Assuming that the power produced by the emission of the sample is negligible, the intensity, I_0 , to the detector is

$$I_0(\nu) [t_{\text{UHMW}}(\nu) + r_{\text{UHMW}}(\nu)] \ll \epsilon_{\text{UHMW}} \cdot BB(T = 300 \text{ K}, \nu), \quad (3)$$

were $BB(T = 300\text{ K})$ is the black body intensity at room temperature, ν is the frequency, t_{UHMW} , r_{UHMW} are the transmissivity and reflectivity of UHMW sample respectively, we can write:

$$\begin{aligned} \frac{S(\nu)}{S'(\nu)} &= \frac{I_0(\nu) [t_{UHMW}(\nu) + r_{UHMW}(\nu)]}{I'_0(\nu)} = \\ &= t_{UHMW}(\nu) + r_{UHMW}(\nu) . \end{aligned} \quad (4)$$

In order to discriminate the transmissivity from the reflectivity, we can use the thickness dependence of the transmissivity for each frequency:

$$\frac{S}{S'} = t_{UHMW} + r_{UHMW} = \left(1 - e^{-d_0/d}\right) + r_{UHMW} . \quad (5)$$

For each frequency, we performed a two-parameter exponential fit of S/S' as function of d , eq. (5), obtaining the values of d_0 and r_{UHMW} . We found a reflectivity less than the 10% for both HDPE and UHMW, and a transmissivity greater than the 90% for the 10 mm thick samples of both materials. Figure 7 shows the transmissivity and the reflectivity for the different samples of HDPE and UHMW. From the top panel of Figure 7 it is possible verify

$$r(\nu) + t(\nu) + \sigma_r(\nu) + \sigma_t(\nu) < 1 \quad \forall \nu$$

so the energy conservation isn't violated.

Since the UHMW is formed by long chains of polyethylene, all aligned in the same direction, the presence of a small residual polarization is possible. Performing different transmissivity measurements by rotating the sample, We did not obtain an evidence of this effect due. However we are preparing dedicated measurements about this. A small effect due to polarization in polymeric materials has been already highlighted in [28].

5. Refractive Index

The last optical property needed for the design of the lenses is the refractive index, which can be measured through a MPI by looking for the *zero path difference* (ZPD) shift due to the passage in a different material. The optical

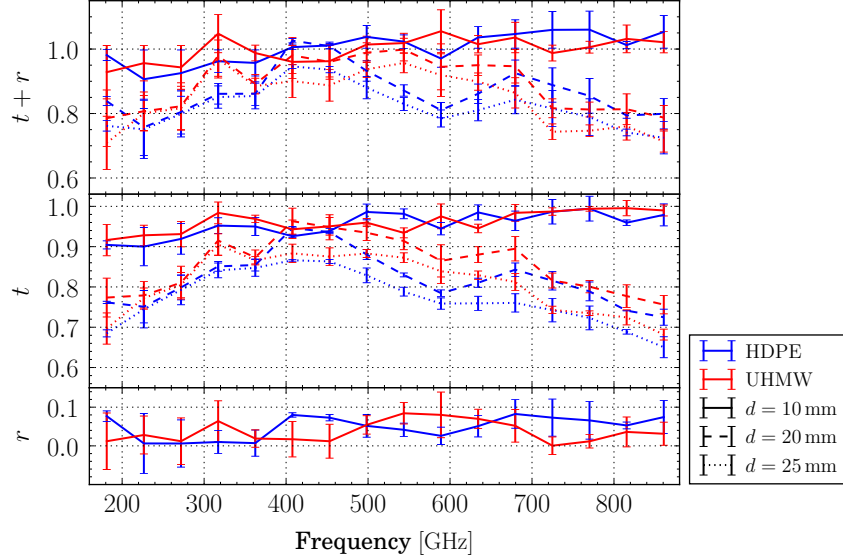


Figure 7: Transmissivity (*central panel*) and reflectivity (*bottom panel*) for the samples of HDPE (*red*) and UHMW (*blue*). The transmissivity is shown for different thicknesses of the samples: 10 (*solid line*), 20 (*dashed line*), and 25 mm (*dotted line*). The *top panel* shows the trend of the sum of the transmissivity and the reflectivity.

shift Δx is proportional to the thickness of the material, d , according to the following equation:

$$\Delta x = (n - 1) d, \quad (6)$$

where n is the real part of the complex refractive index \hat{n} :

$$\hat{n} = n - ik, \quad (7)$$

we can express the imaginary part as a function of absorption parameter α :

$$\alpha = 4\pi f k / c, \quad (8)$$

where f is the frequency, c is the light speed and k is the extinction coefficient.

The HDPE refractive index at millimeter wavelengths is 1.54 [23, 24, 29]. The absorption coefficient in the same range at 300K is $0.03 \text{ Np} \cdot \text{cm}^{-1}$ [23, 24, 29].

5.1. Instrumental setup

The setup is the same described for the transmission measurement, with the sample located between the beam splitter and one of the two roof mirrors. In this way, there is an additional phase shift Δx and, therefore, a different ZPD position. We perform the measurement with 10 cm^{-1} band-pass filter.

5.2. Measurements

We performed a number of measurements on three different thicknesses of the UHMW sample. In Figure 8 is shown a raw measurement of the 10 mm thick sample; each interferogram is performed by around 15 minutes of integration time. From preliminary measurements, we acquired long interferograms, finding raw ZPD positions, then we refined the measurements around the ZPD positions, in order to improve the precision. Tab. 3 summarizes the results for the ZPD shifts and the refractive indexes for the different thicknesses of the UHMW sample, we show also an upper limit for the absorption factor.

Thickness [mm]	$\overline{\Delta x}$ [cm]	$\sigma_{\Delta x}$	n	σ_n	$\alpha[Np \cdot cm^{-1}]$
10	0.539	0.006	1.539	0.008	0.03
20	1.075	0.03	1.54	0.02	0.04
25	1.33	0.03	1.53	0.02	0.03

Table 3: Results for the ZPD shifts and the refractive indexes for the different thicknesses of the UHMW sample at 300 GHz.

Finally, we found the following mean refractive index at 300 GHz:

$$n = 1.537 \pm 0.009 . \quad (9)$$

and the upper limit for the absorption coefficient at 300 GHz:

$$\alpha = 0.03 \pm 0.01 \text{ Np} \cdot \text{cm}^{-1} . \quad (10)$$

The results are compatible with the HDPE [23, 24, 29] and it is compatible with the results obtained in Figure 7 at 300 GHz.

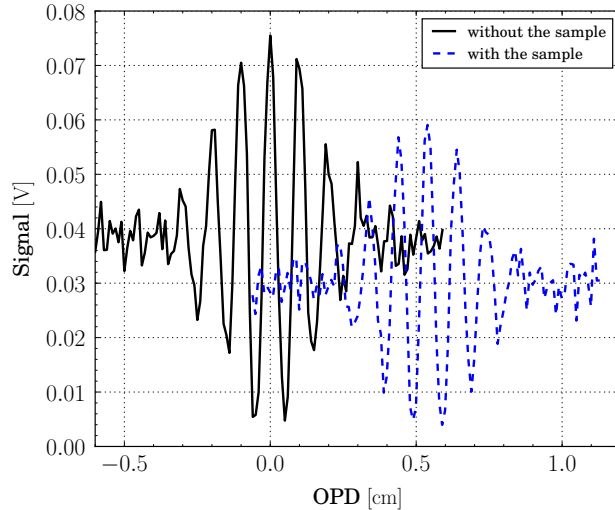


Figure 8: Raw interferogram produced by the difference of two blackbodies (4000 K and 300 K) by using a MPI. The signal is plot as a function of Optical Path Difference (OPD). The *solid black line* represents the interferogram measured without the sample, while the *dashed blue line* represents the interferogram measured with the 10 mm thick sample of UHMW placed on the delay line. The different position of the ZPD is directly dependent on the refractive index of the material according to eq. (6).

6. Conclusion

We perform dedicated measurement in order to put in light the goodness about this material for millimeter wavelength applications. We measured its emissivity at 90 GHz and 150 GHz obtaining few percent, this results are consistent with similar plastic polymer material as the HDPE. By using a MPI and a Golay Cell, as detector, we measured the transmissivity as a function of the thickness. We measure $\sim 90\%$ from 150 GHz to 800 GHz for ten millimeter sheet. From these measure we derive the surface reflectivity, without coating, always less 20%. The results are very similar to HDPE. By using the same MPI as before we measured the refractive index, 1.537, and the absorption coefficient, $0.03Np \cdot cm^{-1}$, both obtained at 300 GHz. The optical feature, very similar to HDPE, and the better mechanical characteristic make this material

very suitable for millimeter wavelengths.

7. Founding

This work has been supported by ASI (Agenzia Spaziale Italiana), grants OLIMPO and Millimetron, by PNRA (Italian National Antarctic Research Program), and by Sapienza University of Rome *research-startup* funds.

8. Acknowledgments

We warmly acknowledge Mr. Giorgio Amico for careful machining of many part of the experiment.

References

References

- [1] S. Masi, P. Ade, P. de Bernardis, A. Boscaleri, M. De Petris, G. De Troia, M. Fabrini, M. Giacometti, A. Iacoangeli, L. Lamagna, A. Lange, P. Lubin, P. Mauskopf, A. Melchiorri, F. Melchiorri, F. Nati, L. Nati, A. Orlando, E. Pascale, F. Piacentini, M. Pierre, G. Polenta, Y. Rephaeli, G. Romeo, D. Yvon, OLIMPO: A few arcmin resolution survey of the sky at mm and sub-mm wavelengths, *Memorie della Società Astronomica Italiana* 74 (2003) 96.
- [2] A. Coppolecchia, Olimpo: A 4-bands detectors array for balloon-borne observations of the sunyaev-zeldovich effect. in: *New horizons for observational cosmology*, Proceeding of Varenna Cosmology confereces 186. doi:10.3254/978-1-61499-476-3-257.
- [3] P. de Bernardis, S. Colafrancesco, G. D'Alessandro, L. Lamagna, P. Marchegiani, S. Masi, A. Schillaci, Low-resolution spectroscopy of the Sunyaev-Zel'dovich effect and estimates of cluster parameters, *Astronomy & Astrophysics* 538 (2012) A86. arXiv:1111.4588, doi:10.1051/0004-6361/201118062.

[4] P. André, C. Baccigalupi, A. Banday, D. Barbosa, B. Barreiro, J. Bartlett, N. Bartolo, E. Battistelli, R. Battye, G. Bendo, A. Benoît, J.-P. Bernard, M. Bersanelli, M. Béthermin, P. Bielewicz, A. Bonaldi, F. Bouchet, F. Boulanger, J. Brand, M. Bucher, C. Burigana, Z.-Y. Cai, P. Camus, F. Casas, V. Casasola, G. Castex, A. Challinor, J. Chluba, G. Chon, S. Colafrancesco, B. Comis, F. Cuttaia, G. D’Alessandro, A. Da Silva, R. Davis, M. de Avillez, P. de Bernardis, M. de Petris, A. de Rosa, G. de Zotti, J. Delabrouille, F.-X. Désert, C. Dickinson, J. M. Diego, J. Dunkley, T. Enßlin, J. Errard, E. Falgarone, P. Ferreira, K. Ferrière, F. Finelli, A. Fletcher, P. Fosalba, G. Fuller, S. Galli, K. Ganga, J. García-Bellido, A. Ghribi, M. Giard, Y. Giraud-Héraud, J. Gonzalez-Nuevo, K. Grainge, A. Gruppuso, A. Hall, J.-C. Hamilton, M. Haverkorn, C. Hernandez-Monteagudo, D. Herranz, M. Jackson, A. Jaffe, R. Khatri, M. Kunz, L. Lamagna, M. Lattanzi, P. Leahy, J. Lesgourgues, M. Liguori, E. Liuzzo, M. Lopez-Caniego, J. Macias-Perez, B. Maffei, D. Maino, A. Mangilli, E. Martinez-Gonzalez, C. J. A. P. Martins, S. Masi, M. Massardi, S. Matarrese, A. Melchiorri, J.-B. Melin, A. Mennella, A. Mignano, M.-A. Miville-Deschênes, A. Monfardini, A. Murphy, P. Naselsky, F. Nati, P. Natoli, M. Negrello, F. Noviello, C. O’Sullivan, F. Paci, L. Pagano, R. Paladino, N. Palanque-Delabrouille, D. Paoletti, H. Peiris, F. Perrotta, F. Piacentini, M. Piat, L. Piccirillo, G. Pisano, G. Polenta, A. Pollo, N. Ponthieu, M. Remazeilles, S. Ricciardi, M. Roman, C. Rosset, J.-A. Rubino-Martin, M. Salatino, A. Schillaci, P. Shellard, J. Silk, A. Starobinsky, R. Stompor, R. Sunyaev, A. Tartari, L. Terenzi, L. Toffolatti, M. Tomasi, N. Trappe, M. Tristram, T. Trombetti, M. Tucci, R. Van de Weijgaert, B. Van Tent, L. Verde, P. Vielva, B. Wandelt, R. Watson, S. Withington, PRISM (Polarized Radiation Imaging and Spectroscopy Mission): an extended white paper, *Journal of Cosmology and Astroparticle Physics* 2 (2014) 006. [arXiv:1310.1554](https://arxiv.org/abs/1310.1554), [doi:10.1088/1475-7516/2014/02/006](https://doi.org/10.1088/1475-7516/2014/02/006).

[5] L. M. Fissel, P. Ade, F. E. Angilè, P. Campbell Ashton, J. E. Austermann,

- T. Billings, G. Che, H.-M. Cho, M. R. Cunningham, K. Davis, M. J. Devlin, S. Dicker, B. Dober, Y. Fukui, N. Galitzki, j. gao, S. Gordon, C. E. Groppi, S. Hillbrand, G. Hilton, H. Hubmayr, K. Irwin, P. Jones, J. Klein, d. li, Z.-Y. Li, n. lourie, I. Lowe, H. Mani, P. G. Martin, P. Mauskopf, C. McKenney, F. Nati, G. Novak, E. Pascale, g. pisano, F. Pereira Santos, D. Scott, A. Sinclair, J. Diego Diego Soler, c. tucker, M. Underhill, M. Visser, P. Williams, BLAST-TNG: A Next Generation Balloon-borne Large Aperture Submillimeter Polarimeter, Vol. 229 of American Astronomical Society Meeting Abstracts, 2017, p. 133.06.
- [6] B. P. Crill, P. A. R. Ade, E. S. Battistelli, S. Benton, R. Bihary, J. J. Bock, J. R. Bond, J. Brevik, S. Bryan, C. R. Contaldi, O. Doré, M. Farhang, L. Fissel, S. R. Golwala, M. Halpern, G. Hilton, W. Holmes, V. V. Hristov, K. Irwin, W. C. Jones, C. L. Kuo, A. E. Lange, C. Lawrie, C. J. MacTavish, T. G. Martin, P. Mason, T. E. Montroy, C. B. Netterfield, E. Pascale, D. Riley, J. E. Ruhl, M. C. Runyan, A. Trangsrud, C. Tucker, A. Turner, M. Viero, D. Wiebe, SPIDER: a balloon-borne large-scale CMB polarimeter, in: Space Telescopes and Instrumentation 2008: Optical, Infrared, and Millimeter, Vol. 7010 of Proceedings of SPIE, 2008, p. 70102P. [arXiv:0807.1548](https://arxiv.org/abs/0807.1548), doi:10.1117/12.787446.
- [7] Schillaci, Alessandro, D'Alessandro, Giuseppe, de Bernardis, Paolo, Masi, Silvia, Novaes, Camila Paiva, Gervasi, Massimo, Zannoni, Mario, Efficient differential fourier-transform spectrometer for precision sunyaev-zeldovich effect measurements, *Astronomy & Astrophysics* 565 (2014) A125. doi:10.1051/0004-6361/201423631. URL <https://doi.org/10.1051/0004-6361/201423631>
- [8] P. de Bernardis, S. Aiola, G. Amico, E. Battistelli, A. Coppolecchia, A. Cruciani, A. D'Addabbo, G. D'Alessandro, S. De Gregori, M. De Petris, D. Goldie, R. Gualtieri, V. Haynes, L. Lamagna, B. Maffei, S. Masi, F. Nati, M. W. Ng, L. Pagano, F. Piacentini, L. Piccirillo, G. Pisano, G. Romeo, M. Salatino, A. Schillaci, E. Tommasi, S. Withington, SWIPE:

a bolometric polarimeter for the Large-Scale Polarization Explorer, Vol. 8452 of Proceedings of SPIE, 2012, p. 84523F. [arXiv:1208.0282](https://arxiv.org/abs/1208.0282), doi: 10.1117/12.926569.

- [9] D. S. Swetz, P. A. R. Ade, C. Allen, M. Amiri, J. W. Appel, E. S. Battistelli, B. Burger, J. A. Chervenak, A. J. Dahlen, S. Das, S. Denny, M. J. Devlin, S. R. Dicker, W. B. Doriese, R. Dnner, T. Essinger-Hileman, R. P. Fisher, J. W. Fowler, X. Gao, A. Hajian, M. Halpern, P. C. Hargrave, M. Hasselfield, G. C. Hilton, A. D. Hincks, K. D. Irwin, N. Jarosik, M. Kaul, J. Klein, S. Knotek, J. M. Lau, M. Limon, R. H. Lupton, T. A. Marriage, K. L. Martocci, P. Mauskopf, S. H. Moseley, C. B. Netterfield, M. D. Niemack, M. R. Nolta, L. Page, L. P. Parker, B. A. Reid, C. D. Reintsema, A. J. Sederberg, N. Sehgal, J. L. Sievers, D. N. Spergel, S. T. Staggs, O. R. Stryzak, E. R. Switzer, R. J. Thornton, C. Tucker, E. J. Wollack, Y. Zhao, Instrument design and characterization of the millimeter bolometer array camera on the atacama cosmology telescope, Proceedings of SPIE 7020 (2008) 702008–702008–12. doi:10.1117/12.789876.

URL <http://dx.doi.org/10.1117/12.789876>

- [10] G. Sui, W. Zhong, X. Ren, X. Wang, X. Yang, Structure, mechanical properties and friction behavior of uhmwpe/hdpe/carbon nanofibers, Materials Chemistry and Physics 115 (1) (2009) 404 – 412. doi:<https://doi.org/10.1016/j.matchemphys.2008.12.016>.

URL <http://www.sciencedirect.com/science/article/pii/S0254058408010018>

- [11] B. Alcock, N. Cabrera, N.-M. Barkoula, J. Loos, T. Peijs, The mechanical properties of unidirectional all-polypropylene composites, Composites Part A: Applied Science and Manufacturing 37 (5) (2006) 716 – 726. doi:<https://doi.org/10.1016/j.compositesa.2005.07.002>.

URL <http://www.sciencedirect.com/science/article/pii/S1359835X05002800>

- [12] J. Sayers, N. G. Czakon, P. K. Day, T. P. Downes, R. P. Duan, J. Gao, J. Glenn, S. R. Golwala, M. I. Hollister, H. G. LeDuc, B. A. Mazin, P. R. Maloney, O. Noroozian, H. T. Nguyen, J. A. Schlaerth, S. Siegel, J. E. Vaillancourt, A. Vayonakis, P. R. Wilson, J. Zmuidzinas, Optics for MUSIC: a new (sub)millimeter camera for the Caltech Submillimeter Observatory, Proceedings of SPIE 7741 (2010) 77410W. doi:10.1117/12.857324.
- [13] M. Velázquez, D. Ferrusca, E. Castillo-Dominguez, E. Ibarra-Medel, S. Ventura, V. Gómez-Rivera, D. Hughes, I. Aretxaga, W. Grant, M. Doyle, S., Design of a 2-mm wavelength kids prototype camera for the large millimeter telescope, Journal of Low Temperature Physics 184 (3) (2016) 799–804. doi:10.1007/s10909-016-1536-6.
URL <http://dx.doi.org/10.1007/s10909-016-1536-6>
- [14] E. S. Battistelli, G. Amico, A. Baù, L. Bergé, É. Bréelle, R. Charlassier, S. Collin, A. Cruciani, P. de Bernardis, C. Dufour, L. Dumoulin, M. Gervasi, M. Giard, C. Giordano, Y. Giraud-Héraud, L. Guglielmi, J.-C. Hamilton, J. Landé, B. Maffei, M. Maiello, S. Marnieros, S. Masi, A. Passerini, F. Piacentini, M. Piat, L. Piccirillo, G. Pisano, G. Polenta, C. Rosset, M. Salatino, A. Schillaci, R. Sordini, S. Spinelli, A. Tartari, M. Zannoni, Intensity and polarization of the atmospheric emission at millimetric wavelengths at Dome Concordia, Monthly Notices of the Royal Astronomical Society 423 (2012) 1293–1299. arXiv:1203.5615.
- [15] T. Essinger-Hileman, A. Ali, M. Amiri, J. W. Appel, D. Araujo, C. L. Bennett, F. Boone, M. Chan, H.-M. Cho, D. T. Chuss, F. Colazo, E. Crowe, K. Denis, R. Dünner, J. Eimer, D. Gothe, M. Halpern, K. Harrington, G. C. Hilton, G. F. Hinshaw, C. Huang, K. Irwin, G. Jones, J. Karakla, A. J. Kogut, D. Larson, M. Limon, L. Lowry, T. Marriage, N. Mehrle, A. D. Miller, N. Miller, S. H. Moseley, G. Novak, C. Reintsema, K. Rostem, T. Stevenson, D. Towner, K. U-Yen, E. Wagner, D. Watts, E. J. Wollack, Z. Xu, L. Zeng, CLASS: the cosmology large angular scale surveyor, Vol.

9153 of Proceedings of SPIE, 2014, p. 91531I. [arXiv:1408.4788](#), [doi:10.1117/12.2056701](#).

- [16] A. Schillaci, E. Battistelli, G. D' Alessandro, P. de Bernardis, S. Masi, On the emissivity of wire-grid polarizers for astronomical observations at mm-wavelengths, *Infrared Physics and Technology* 58 (2013) 64–68. [arXiv:1212.3969](#), [doi:10.1016/j.infrared.2013.01.009](#).
- [17] F. L. Bock JJ., Parikh MK., Emissivity measurements of reflective surfaces at near-millimeter wavelengths, *Applied Optics* 34 (1995) 4812–4816.
- [18] Mark Halpern, Herbert P. Gush, Edward Wishnow, Vittorio De Cosmo, Far infrared transmission of dielectrics at cryogenic and room temperatures: glass, fluorogold, eccosorb, stycast, and various plastics, *Applied Optics* 25 (4) (1986) 565–570. [doi:10.1364/AO.25.000565](#).
URL <http://ao.osa.org/abstract.cfm?URI=ao-25-4-565>
- [19] B. Mazin, Microwave kinetic inductance detectors, Ph.D. thesis, California Institute of Technology (2005).
- [20] S. Doyle, Lumped element kinetic inductance detectors, Ph.D. thesis, Cardiff University (2008).
- [21] I. Colantoni, F. Bellini, L. Cardani, N. Casali, M. G. Castellano, A. Coppolecchia, C. Cosmelli, A. Cruciani, A. D'Addabbo, S. Di Domizio, M. Martinez, C. Tomei, M. Vignati, Design and fabrication of the kid-based light detectors of calder, *Journal of Low Temperature Physics* 184 (1) (2016) 131–136. [doi:10.1007/s10909-015-1452-1](#).
URL <http://dx.doi.org/10.1007/s10909-015-1452-1>
- [22] A. Paiella, A. Coppolecchia, M. G. Castellano, I. Colantoni, A. Cruciani, A. D'Addabbo, P. de Bernardis, S. Masi, G. Presta, Development of lumped element kinetic inductance detectors for the w-band, *Journal of Low Temperature Physics* 184 (1) (2016) 97–102. [doi:10.1007/](#)

s10909-015-1470-z.

URL <http://dx.doi.org/10.1007/s10909-015-1470-z>

- [23] J. Lamb, Miscellaneous data on materials for millimetre and submillimetre optics, *International Journal of Infrared and Millimeter Waves* 17 (1996) 1997–2034. doi:10.1007/BF02069487.
- [24] E. Hemmati H., Mather J.C., Submillimeter and millimeter wave characterization of absorbing materials, *Applied Optics* 24 (1985) 4489–4492. doi:10.1364/AO.24.004489.
- [25] G. D’Alessandro, P. de Bernardis, S. Masi, A. Schillaci, Common-mode rejection in Martin-Puplett spectrometers for astronomical observations at millimeter wavelengths, *Applied Optics* 54 (2015) 9269. arXiv:1509.09221, doi:10.1364/AO.54.009269.
- [26] G. D’Alessandro, P. de Bernardis, S. Di Tano, S. Masi, L. Mele, Beam splitter orientation error in martin-pupplet interferometer for millimeter wave spectroscopy, *Infrared Physics Technology* 85 (2017) 92–98. doi:10.1016/j.infrared.2017.05.015.
- [27] G. D’Alessandro, P. de Bernardis, S. Masi, A. Schillaci, Development of instrumentation for differential spectroscopic measurements at millimeter wavelengths, *Proceedings of SPIE* 9914 (2016) 99143N–99143N–17. doi:10.1117/12.2238504.
URL <http://dx.doi.org/10.1117/12.2238504>
- [28] G. Coppi, T. Marchetti, P. de Bernardis, S. Masi, Measurements of the polarization properties of foam materials useful for mm-wave polarimeters windows, *Journal of Infrared, Millimeter, and Terahertz Waves* 37 (8) (2016) 815–824. doi:10.1007/s10762-016-0272-y.
URL <https://doi.org/10.1007/s10762-016-0272-y>
- [29] J. Birch, J. Dromey, J. Lesurf, The optical constants of some common low-loss polymers between 4 and 40 cm⁻¹, *Infrared Physics* 21 (4) (1981)

225 – 228. doi:[https://doi.org/10.1016/0020-0891\(81\)90053-1](https://doi.org/10.1016/0020-0891(81)90053-1).

URL [http://www.sciencedirect.com/science/article/pii/0020089181900531](http://www.sciencedirect.com/science/article/pii/S0020089181900531)